ULUSLARARASI 3B YAZICI TEKNOLOJİLERİ
VE DİJİTAL ENDÜSTRİ DERGİSİ

INTERNATIONAL JOURNAL OF 3D PRINTING TECHNOLOGIES AND DIGITAL INDUSTRY

ISSN:2602-3350 (Online)

URL: https://dergipark.org.tr/ij3dptdi

EVALUATION OF U-Net AND ResNet ARCHITECTURES FOR BIOMEDICAL IMAGE SEGMENTATION

Yazarlar (Authors): Mücahit Çalışan *, Veysel Gündüzalp, Nevzat Olgun

Bu makaleye şu şekilde atıfta bulunabilirsiniz (To cite to this article): *Çalışan M., Gündüzalp V., Olgun N., "Evaluation of U-Net and ResNet Architectures for Biomedical Image Segmentation" Int. J. of 3D Printing Tech. Dig. Ind., 7(3): 561-570, (2023).*

DOI: 10.46519/ij3dptdi.1366431

Araştırma Makale/ Research Article

Erişim Linki: (To link to this article): https://dergipark.org.tr/en/pub/ij3dptdi/archive

EVALUATION OF U-Net AND ResNet ARCHITECTURES FOR BIOMEDICAL IMAGE SEGMENTATION

Mücahit Çalışan [a]*, Veysel Gündüzalp [b], Nevzat Olgun [c]

[a]Bingöl University, Engineering and Architecture Faculty, Department of Computer Engineering, TÜRKİYE
[b]İnönü University, Engineering Faculty, Department of Computer Engineering, TÜRKİYE
[c]Afyon Kocatepe University, Technology Faculty, Department of Software Engineering, TÜRKİYE

* *Corresponding Author:* mcalisan@bingol.edu.tr

(**Received:** 26.09.23; **Revised:** 08.11.23; **Accepted:** 24.11.23)

ABSTRACT

Medical professionals need methods that provide reliable information in diagnosing and monitoring neurological diseases. Among such methods, studies based on medical image analysis are essential among the active research topics in this field. Tumor segmentation is a popular area, especially with magnetic resonance imaging (MRI). Early diagnosis of tumours plays an essential role in the treatment process. This situation also increases the survival rate of the patients. Manually segmenting a tumour from MR images is a difficult and time-consuming task within the anatomical knowledge of medical professionals. This has necessitated the need for automatic segmentation methods. Convolutional neural networks (CNN), one of the deep learning methods that provide the most advanced results in the field of tumour segmentation, play an important role. This study, tumor segmentation was performed from brain and heart MR images using CNN-based U-Net and ResNet50 deep network architectures. In the segmentation process, their performance was tested using Dice, Sensitivity, PPV and Jaccard metrics. High performance levels were sequentially achieved using the U-Net network architecture on brain images, with success rates of approximately 98.47%, 98.1%, 98.85%, and 96.07%

Keywords: Tumor Segmentation, Magnetic Resonance Imaging, MRI, Deep Learning, Glioma

1. INTRODUCTION

Uncontrolled growth and division of cells in the body are extremely dangerous for human life. These unnatural growths and divisions are called tumours. The most common significant tumours in adult humans are gliomas [1]. According to the World Health Organization (WHO), gliomas classified as pathologically low-grade and high-grade are fatal. Low-grade gliomas (LGG) and high-grade gliomas (HGG) are included in the WHO grading class [2]. Particularly when considering the mortality rate of the HGG class, it poses a significant threat to human health. The average survival time for a patient in the HGG class is less than two years [3]. LGG tends to grow more slowly and often presents as benign. However, there is a potential for them to transform into HGG over time. LGG and HGG require neuroimaging in surgical planning and treatment[4].

Early diagnosis of gliomas is essential in improving people's treatment processes. However, unreliable segmentation during the identification of gliomas may leave undesirable consequences on treatment and surgery. Different imaging techniques provide valuable information about gliomas' shapes, locations and metabolism. Computed tomography (CT), Positron emission tomography (PET), and Magnetic resonance imaging (MRI) are among the main imaging techniques. MRI has become a standard technique for tumour diagnosis due to its soft tissue contrast and availability. This technique uses radio frequency signals and has a strong magnetic field effect to stimulate target tissues. The MRI imaging method does not cause injuries and provides high-quality images without leaving unwanted damage on sensitive areas such as the skull. MRI also allows multiple imaging to obtain different structures of a tissue.

Due to the structural complexity of gliomas, different image types provide complementary information to analyze different glioma sub-regions. For example, T1, T1C, T2 and FLAIR areas in skull MR images consist of brain tissues with different contrast variations. T1 images show anatomy, while T2 images show pathology. FLAIR shows the borders of the brain tumor.

Innovations in computer vision and image processing make a significant contribution to the detection of tumours. Accurate information about the disease using new techniques and algorithms contributes to early diagnosis. Convolutional Neural Networks (CNN) are central to these advanced techniques and algorithms. With the emergence of CNNs, a leap has been seen in medical image analysis in recent years [5]. The most important of the main difficulties encountered in medical image analysis is detecting the desired area in the images. Detecting these areas has become a prerequisite for many different clinical applications. Brain tumor segmentation [6], prostate tumour segmentation [7], abdominal organ tumour segmentation [8], and cell segmentation are the main clinical applications. Identifying the brain tumor in this segmentation diversity is of particular importance. The variation in the shape and size of brain tumor areas further complicates the segmentation process. Additional difficulties in brain tumor segmentation are the location of the tumor and the fact that the tumor contains heterogeneous tissue. These difficulties in MR image analysis have led many researchers to find suitable segmentation methods. Manual segmentation is time consuming and cannot be applied to 3D MR images. Automatic tumour segmentation is one of the challenges due to the intertwining of the tumor and surrounding tissue. Therefore, researchers have always focused on finding the right methods for automatic segmentation.

Classical machine learning algorithms use features extracted from the dataset. These features are given to classification algorithms such as Support Vector Machines (SVM) [9], Fuzzy C-Means algorithm [10], and Random Forest [11]. Mathew et al. used discrete wavelet transform to extract features from MR images for brain tumor detection. They used SVM for tumor segmentation and classification with the obtained features [12]. Kailash D. Kharat et al. proposed artificial neural networks to classify MRI images [13]. Eman Abdel-Maksoud et al. used the K-means clustering technique integrated with the Fuzzy C-means algorithm [14]. Pinto et al. entered the BRATS 2013 list for glioma segmentation with a method based on an Extreme Random Forest [15]. However, these methods generally have limited representation ability for accurate recognition.

In recent years, successful performances have been obtained for medical image segmentation with deep learning-based methods. The use of low-cost GPUs has led many researchers to CNNs. Self-learning and generalisation capabilities on big data have made CNNs popular in this field [16-17]. There are 2D and 3D network approaches according to the size of the information given to the CNN. In terms of efficiency, 2D networks are more effective. 3D networks can directly process 3D MR images. However, it requires more GPU and computational cost. Chen et al. adopted the Residual network idea, which differs from the networks constructed only by successive addition of convolutional layers [18]. Wang et al. proposed a cascaded and fully convolutional neural network for medical image segmentation [19]. Idanis Diaz et al. developed a method that separates different components of a brain tumor [20]. The method was applied to four types of MR imaging to find the tumour volume. Morphological operations such as the histogram thresholding technique and geodesic transformations are also used. Jin Liu et al. presented a comprehensive overview of MRI-based segmentation methods [21]. Chen et al. presented three different convolution networks [22]. Each network was trained with 3D segments as input for the segmentation target. Histogram equalisation and voxel normalisation were performed on the segments. Dong et al. presented a model for augmenting the data, but they could not segment low-grade gliomas for segmentation [23]. Myronenko presented an encoder-decoder architecture and added another decoder layer to recover the input image [24]. Lachinov trained multiple 3D U-Net networks in a cascade to segment tumour sub-regions sequentially [25]. Ronneberger et al. used the U-Net network, an encoder-decoder network architecture, in medical image segmentation, which requires a deeper network and a larger training set [26].

The limited amount of labelled data, expensive and time-consuming medical image collection, and the need for fast end-to-end modelling have led us to architectures such as U-Net. U-Net architecture makes significant contributions to biomedical image segmentation with CNNs. This architecture has become popular for successfully segmenting images with limited labelled training data. In this architecture, as the number of layers increases, it learns more representative features, and its performance increases even more. The increase in the number of layers of the network also increases the number of parameters that enable the network to learn features. The increase in the number of parameters also increases the difficulties in training the network.

In this study, parameter optimisation was performed to improve the performance of U-Net and ResNet50 on medical image segmentation. These architectures were used for tumour detection in brain and heart MR images by optimising the parameters. The network structure was tested on MRI data sets.

2. MATERIAL AND METHOD

The main methodology of the study is to take MR images of different tissues as input and provide a segmentation mask as output. A summary of the methodology consisting of MRI preprocessing, trained weights, architecture used and tumour segmentation steps is given in Figure 1. Firstly, the data set used in the study is defined, and then the methods used are presented with explanations. The results obtained after training the network architectures are compared with other studies in the literature.

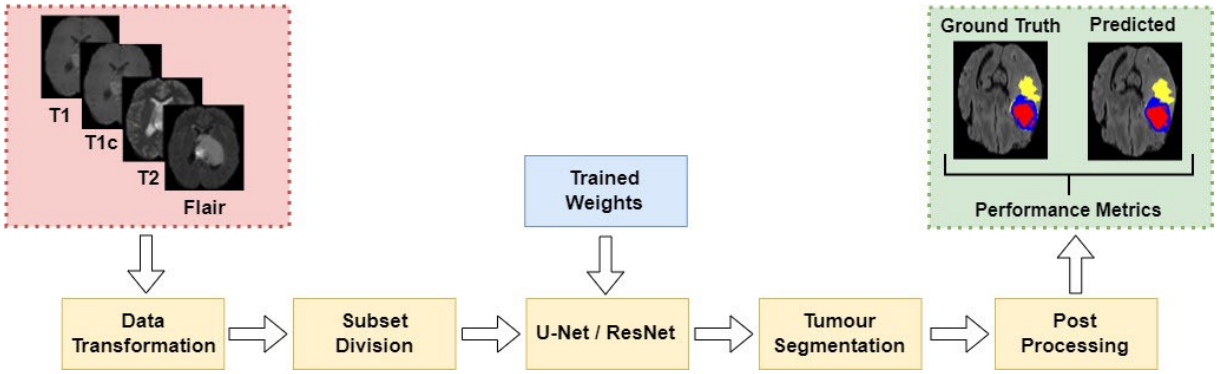

Figure 1. Block diagram of the methodology used in the study

2.1. Description of Data Sets

Segmentation of medical images aims to associate the image with relevant labels without human interaction. When the labels provided by experts are combined with imaging data, the success of the segmentation methods is revealed. Various medical imaging clusters available in open access are helping to improve segmentation algorithms.

Table 1. Medical image datasets used in the study

Data	Type	Image sequence	Labels
Brain Tumours [27-28]	MRI	T1, T1c, T2, Flair	edema, non-enhancing tumour, enhancing tumour
Heart [27-28]	MRI	3D	left atrium

In this study, two different data sets consisting of brain and heart MR images were used. The main information about the data sets used in the study is given in Table 1.

2.1.1. Brain data set

The Brain tumor Segmentation 2015 (BRATS) dataset, which consists of brain MR images, contains data from 750 patients. Brain tumors, usually low-contrast, are difficult to separate from c brain tissue. This problem can be overcome with MRI-scanned images with multiple parameters. The brain MRI data of each patient consists of 4 image sequences. These sequences with different characteristics consist of radio frequency pulse, gradient and signal collection processes. These are T1-weighted (T1), contrast-enhanced T1-weighted (T1c), T2-weighted (T2) and Flair. Using short-timed radio frequencies, T1 makes the image appear brighter due to the contrast material. In

T2, which uses long-timed radio frequencies, contrast and brightness are determined according to the characteristics of the tissue. Flair images, which use longer timing radio frequencies, are similar to T2, but the image is darker. For each image sequence, the image size was obtained as 240 (horizontal slice) x 240 (vertical slice) x 155 (number of slices). The images have a voxel resolution of 1×1×1×1 mm^3. An example of brain MR images consisting of T1, T1c, T2 and Flair are given in Figure 2.

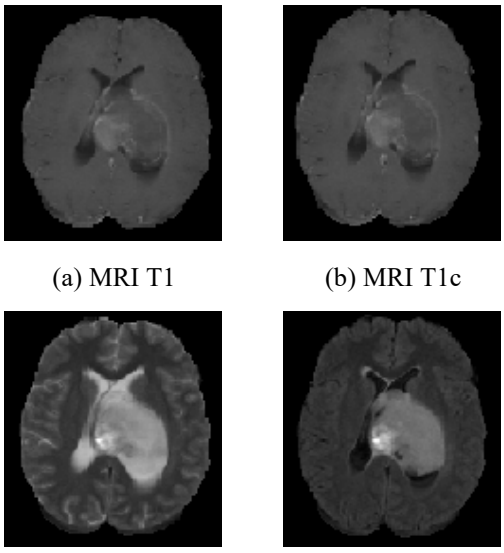

(a) MRI T1 (b) MRI T1c

(c) MRI T2 (d) MRI Flair

Figure 2. Example MRI sequence of the BRATS dataset

2.1.2. Heart data set

A preoperative CT or MRI scan is recommended for most patients to obtain an anatomical representation of the Left Atrial. Accurate anatomical representation of the Left Atrial is crucial to the success of the intervention. The cardiac data set created for automatic segmentation purposes includes 30 MR images scanned in a single cardiac procedure covering the entire heart. The images have a voxel resolution of 1.25×1.25×2.7 mm^3. This dataset was chosen due to its combination of a small training dataset with large anatomical variability. During the data set preparation process, experts performed manual segmentation. Sample MR images of the heart dataset called Left Atrial Segmentation Challenge (LASC) are given in Figure 3.

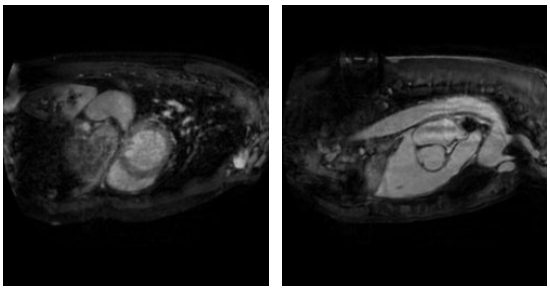

Figure 3. Example heart MRI

2.2. Method

In this study, tumour segmentation was performed using U-Net and ResNet50 architectures. Both architectures are based on a convolutional network architecture. In these architectures, user interaction is not required for tumor segmentation. The data set is split into training and test data in deep learning architectures. The designed deep learning architecture is trained on the training data set. With the parameters obtained as a result of the training, the network is expected to make predictions from the test set. For this purpose, the data sets used in the study are split into training, validation and test data, as shown in Table 2.

Table 2. Experimental dataset

Dataset	Training	Validation	Test	Total
Brain	387	97	266	750
Heart	16	4	10	30

The images used in the study are in the neuroimaging informatics technology initiative (NIfTI) format. Images were reformatted to improve consistency and interoperability across all datasets. These formatted images were normalised. Normalised images were used in the training and testing of network architectures. The normalised images are subjected to essential pre-processing steps such as noise removal by applying mathematical operations. Z-score was applied to the images in the data set to reduce intensity variance between MR images.

$$I_{norm} = \frac{I - \mu(I)}{\sigma(I)} \quad (1)$$

In Equation 1, μ and σ represent the mean value and standard deviation of image I, respectively. All experimental studies were performed with Keras. Both architectures in this study are trained by back-propagation and Adam optimiser methods [29]. The Adam optimisation method generally uses the first and

second moments to update the mean of the available gradients. All weights are normally distributed with mean 0 and standard deviation 0.01. The learning rate was set as 0.0001, and the maximum number of epochs was set as 100.

2.2.1. U-Net Architecture

The U-Net architecture, one of the two models used in the study, is based on sub-sampling and upsampling [30]. Sub-sampling (coding) is used for advanced features such as feature extraction and tumour detection. Upsampling (decoding) is used to reconstruct features such as exact positioning and tumour boundaries. Upsampling and sub-sampling methods are symmetric.

The sub-sampling stage with five blocks has 3x3 convolutional layers and 2x2 max-pooling layers. The number of feature maps is increased from 1 to 1024. With the pooling process, the size of the feature map is reduced from 240x240 to 15x15.

In the upsampling stage, each block contains two convolutional layers and one upsampling layer. The size of the feature map is increased from 15x15 to 240x240. Finally, the number of feature maps is reduced to 2 by using a 1x1 convolutional layer. ReLu activation function is used after each convolutional layer [31]. The diagram of the U-Net structure used in the study is given in Figure 4.

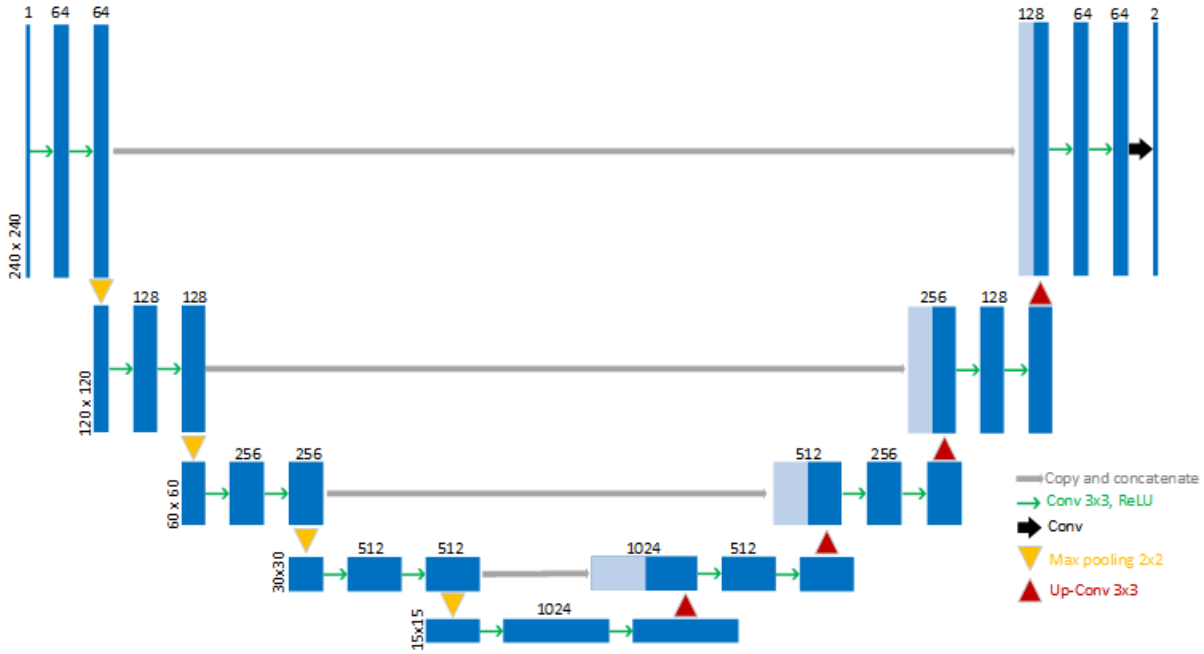

Figure 4. U-Net architecture used in the study

2.2.2. ResNet50 Architecture

Residual Neural Network (ResNet) was developed to reduce the difficulty in training networks with many layers [32]. This model is an enhanced version of CNNs. There are several variants of the model with different weight layers. In this study, ResNet50 architecture consisting of 50 layers is used. ResNet consists of five convolutional blocks. These blocks consist of 1x1, 3x3 and 1x1 convolution layers. The ResNet50 architecture consists of convolution, activation, pooling and fully-Connected layers. ResNet uses a skip connection in which an original input is added to the convolution block's output. The aim here is to reduce the vanishing gradient problem. In the pooling process at the network's end, the average value in each feature map is transferred to the next layer. The detailed diagram of the ResNet50 structure used in the study is given in Figure 5.

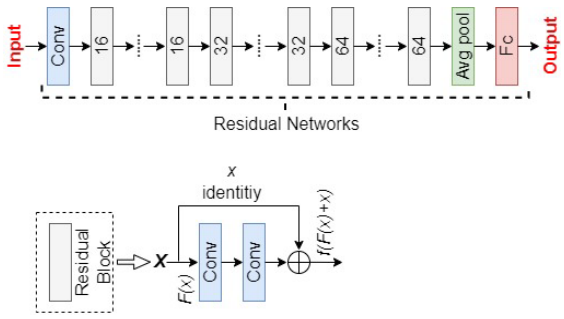

Figure 5. ResNet50 architecture used in the study

3. EXPERIMENTAL RESULTS

MR images in the brain dataset used in the study consist of 4 labels. These are background, edema, non-enhancing tumour and enhancing tumour. MR images in the heart dataset consist of background and left atrium labels.

The training data were trained using different batch sizes and learning rates to investigate the effect of network parameters. When the batch size is 12, U-Net architecture shows better segmentation performance in a shorter time than ResNet50 architecture. Similarly, the best results were obtained with a learning rate of 0.001. The hyperparameters used in both architectures are shown in Table 3.

Table 3. Hyperparameters of the network used in the study

Stage	Hyperparameters	Value
Training	Epoch	50
	Batch size	12
Adam optimizer	$\beta 1$	0.9
	$\beta 2$	0.999
	epsilon	1e-07
	Learning rate	0.001

Three segmentation metrics are considered to evaluate the performance of the architectures on two different data sets. These are Dice Similarity Coefficient (DSC), Positive Predictive Value (PPV) and Sensitivity metrics [32,33]. DSC measures the similarity of segmentation results with manually defined brain regions. Sensitivity measures how well a model can detect positive examples. The sensitivity is calculated as the number of true positives divided by the total number of positives. The performance metrics are defined in Equation 2, Equation 3, and 4, respectively.

$$DSC = \frac{2TP}{FP + 2TP + FN} \quad (2)$$

$$Sensitivity = \frac{TP}{TP + FN} \quad (3)$$

$$PPV = \frac{TP}{TP + FP} \quad (4)$$

In the equations, in the accuracy performance measurement calculation, TP represents the number of true positives, FP indicates the number of false positives, and FN indicates the number of false negatives. In addition to these performance metrics, the Jaccard score was also used in the study. Jaccard score is the most popular performance metric used in medical image segmentation and is defined in Equation 5 [34].

$$Jaccard = \frac{TP}{TP + FP + FN} \quad (5)$$

These performance metrics comprehensively evaluate the segmentation performance. Dice, Sensitivity, PPV and Jaccard score segmentation performance results of U-Net and ResNet50 models are given in Table 4 and Table 5.

Table 4. Brain dataset segmentation performance of U-Net and ResNet50 architectures

Method	Perf. metrics	L1	L2	L3
U-Net	Dice	**0.9847**	**0.9800**	0.8779
ResNet50		0.9328	0.9145	**0.8856**
U-Net	Sensitivity	**0.9810**	**0.9606**	0.8488
ResNet50		0.9367	0.9267	**0.8537**
U-Net	PPV	**0.9885**	**0.9901**	**0.9090**
ResNet50		0.9158	0.9434	0.8812
U-Net	Jaccard	**0.9607**	**0.9517**	**0.7824**
ResNet50		0.9371	0.8769	0.7345

Table 4 shows the performance of U-Net and ResNet50 architectures for the Brain dataset according to different metrics. Column headings L1, L2, and L3 represent edema, non-enhancing tumour and enhancing tumour regions respectively.

Table 5. Heart dataset segmentation performances of U-Net and ResNet50 architectures

Perf. Metrics	Method	
	U-Net	ResNet50
Dice	0.9653	**0.9692**
Sensitivity	0.9282	**0.9627**
PPV	**0.9856**	0.9758
Jaccard	0.9163	**0.9402**

Table 5 shows the performance of U-Net and ResNet50 architectures for the heart dataset according to different metrics.

The results show that the U-Net architecture achieves better segmentation performance than the ResNet50 architecture for brain tumour sub-regions. The heart tumour dataset generally shows that the ResNet50 architecture produces more successful results than the U-Net architecture. The U-Net architecture segmentation results obtained for two different

image sequences in the brain MRI dataset are shown in Figure 6. The segmentation results produced with U-Net are shown in the FLAIR sequence. The U-Net architecture segmentation results obtained for two different image sequences in the heart MRI dataset are shown in Figure 7. The estimation results agree with the manual definition made by experts, referred to as ground truth. However, U-Net may incorrectly identify some complex areas as target tumours.

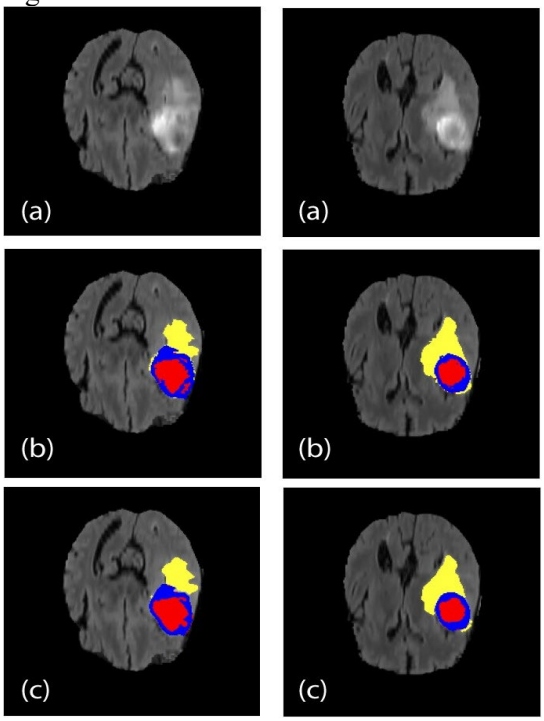

Figure 6. Examples of multi-class brain MR images. a) Original images, b) Ground truth images, c) Segmentation images. Different colours represent different tumour regions: edema (yellow), non-enhancing tumour (blue+red) and enhancing tumour (blue).

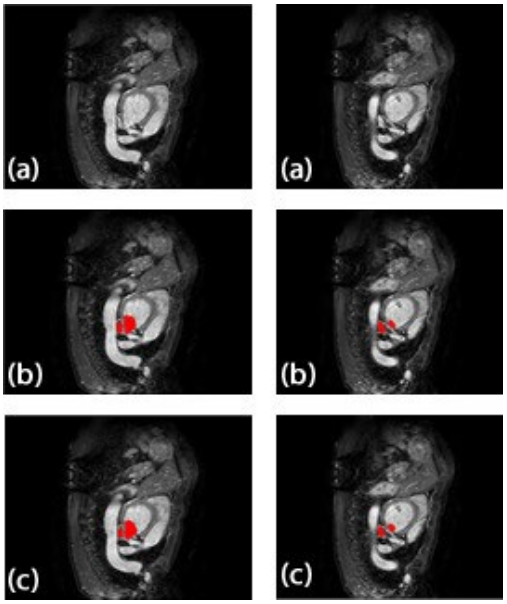

Figure 7. Heart MR image examples. a) Original images, b) Ground truth images, c) Segmentation images.

A brief summary and comparison of similar studies on the segmentation of brain and heart tumours from MR images are given in Table 6. The results of our proposed fully automatic brain tumour segmentation method are compared with the results of other recently published deep learning-based methods. DSC similarity success rates for three subregions of brain and left atrium subregions of heart tumour are given in Table 6. The success of the proposed method was higher than that of the existing methods.

Table 6. Performance comparison of the proposed method with existing methods

Study	Dataset	Dice Similarity Coefficient			
		Brain edema	Brain non-enhancing tumour	Brain enhancing tumour	Heart left atrium
Dong et al. [23]	BRATS 2015	0.88	0.87	0.81	-
Havaei et al. [35]	BRATS 2013	0.88	0.79	0.73	-
Kamnitsas et al. [36]	BRATS 2015	0.90	0.76	0.73	-
Shreyas et al. [37]	BRATS 2015	0.83	0.75	0.72	-
Kong et al. [38]	BRATS 2015	0.90	0.71	0.78	-
Chen et al.[39]	BRATS 2015	0.84	0.69	0.64	-
Tan et al. [40]	BRATS 2015	0.93	0.96	0.84	-
Kausar et al. [41]	LASC 2013	-	-	-	0.84
Chakravarty et al [42]	LASC 2013	-	-	-	0.92
Proposed	**BRATS 2015 LASC 2013**	**0.98**	**0.98**	**0.87**	**0.96**

4. DISCUSSION AND CONCLUSIONS

Biomedical image segmentation is essential in disease diagnosis, treatment planning and subsequent evaluations. With the increase in big biomedical data, the work of specialists in the field, especially neurologists, takes more time. With deep learning-based methods, experts' workload has been reduced and faster and more accurate results have been obtained. This paper presents several deep learning-based methods for automatic MRI tumour segmentation for different input images using fully convolutional networks. The U-Net architecture obtained 98.5%, 98.0% and 87.8% of dice scores for edema, non-enhancing tumour and enhancing tumour in the BRATS dataset, respectively. With the U-Net architecture, a dice success rate of 96.5% was obtained on the heart data set. Extensive experiments are presented on both datasets used. The segmentation performances of the architectures used in the study are presented quantitatively (Table 5,6) and visually (Figure 6,7). The methods' effect was verified with different batch sizes and learning rates. The results show that better segmentation performance is achieved for a batch-size of 12 and a learning rate of 0.001. The proposed methods allow automatic segmentation of the tumour region without manual intervention.

In the future, deep learning-based approaches can be generalised to various organ and lesion segmentation problems. In addition to MRI, more successful results can be obtained with complementary information from different imaging modalities such as Positron Emission Tomography (PET), Man Resonance Spectroscopy (MRS).

REFERENCES

1. Ostrom, Q. T. et al., "CBTRUS Statistical Report: Primary brain and other central nervous system tumors diagnosed in the United States in 2010-2014", Neuro Oncol, Vol. 9, Issue 5, Pages 1– 88, 2017.

2. Soltaninejad, M. et al., "Automated brain tumour detection and segmentation using superpixel-based extremely randomized trees in FLAIR MRI", Int J Comput Assist Radiol Surg, Vol. 12, Issue 2, Pages 183–203, 2017.

3. Louis, D. N. et al., "The 2007 WHO classification of tumours of the central nervous system", Acta Neuropathologica, 114, Pages 97–109, 2007.

4. Menze, B. H. et al., "The Multimodal Brain Tumor Image Segmentation Benchmark (BRATS)", IEEE Trans Med Imaging, Vol. 34, Issue 10, Pages 1993–2024, 2015.

5. Greenspan, H., Van Ginneken, B. & Summers, R. M., "Guest Editorial Deep Learning in Medical Imaging: Overview and Future Promise of an Exciting New Technique", IEEE Transactions on Medical Imaging, Vol. 35, Issue 5, Pages 1153–1159, 2016.

6. De Brébisson, A. & Montana, G., "Deep neural networks for anatomical brain segmentation", IEEE Computer Society Conference on Computer Vision and Pattern Recognition Workshops, Boston, Pages 20–28, 2015.

7. Tian, Z., Liu, L., Zhang, Z. & Fei, B., "PSNet: prostate segmentation on MRI based on a convolutional neural network", Journal of Medical Imaging, Vol. 5, Issue 2, Pages 021208-021208, 2018.

8. Avendi, M. R., Kheradvar, A. & Jafarkhani, H., "A combined deep-learning and deformable-model approach to fully automatic segmentation of the left ventricle in cardiac MRI", Med Image Anal, Vol. 30, Pages 108–119, 2016.

9. Bauer, S., Nolte, L. P. & Reyes, M., "Fully Automatic Segmentation of Brain Tumor Images Using Support Vector Machine Classification in Combination with Hierarchical Conditional Random Field Regularization", Lecture Notes in Computer Science (including subseries Lecture Notes in Artificial Intelligence and Lecture Notes in Bioinformatics), Toronto, Pages 354-361, 2011.

10. Caldairou, B., Passat, N., Habas, P. A., Studholme, C. & Rousseau, F., "A non-local fuzzy segmentation method: Application to brain MRI", Pattern Recognition, Vol. 44, Issue 9, Pages 1916-1927, 2011.

11. Zikic, D. et al., "Decision forests for tissue-specific segmentation of high-grade gliomas in multi-channel MR", Lecture Notes in Computer Science (including subseries Lecture Notes in Artificial Intelligence and Lecture Notes in Bioinformatics), Nice, Pages 369-376, 2012.

12. Mathew, A. R. & Anto, P. B., "Tumor detection and classification of MRI brain image using wavelet transform and SVM", Proceedings of IEEE International Conference on Signal Processing and Communication, ICSPC 2017, Coimbatore Pages 75–78, 2017.

13. Kailash D. Kharat, Pradyumna P. Kulkarni, M. B. N., "Brain Tumor Classification Using Neural Network Based Methods", International Journal of

Computer Science and Informatics, Vol. 1, Issue 2, Pages 2231–5292, 2012.

14. Abdel-Maksoud, E., Elmogy, M. & Al-Awadi, R, "Brain tumor segmentation based on a hybrid clustering technique", Egyptian Informatics Journal, Vol. 16, Issue 1, Pages 71–81, 2015.

15. Pinto, A., Pereira, S., Rasteiro, D. & Silva, C. A., "Hierarchical brain tumour segmentation using extremely randomized trees", Pattern Recognit, Vol. 82, Pages 105–117, 2018.

16. Akkus, Z., Galimzianova, A., Hoogi, A., Rubin, D. L. & Erickson, B. J., "Deep Learning for Brain MRI Segmentation: State of the Art and Future Directions", Journal of Digital Imaging, Vol. 30, Pages 449–459, 2017.

17. Wang, S. H., Sun, J., Phillips, P., Zhao, G. & Zhang, Y. D., "Polarimetric synthetic aperture radar image segmentation by convolutional neural network using graphical processing units", Journal of Real-Time Image Processing, Vol. 15, Pages 631–642, 2018.

18. Chen, H., Dou, Q., Yu, L., Qin, J. & Heng, P. A., "VoxResNet: Deep voxelwise residual networks for brain segmentation from 3D MR images", NeuroImage, Vol. 170, Pages 446–455, 2018.

19. Wang, G., Li, W., Ourselin, S. & Vercauteren, T., "Automatic brain tumor segmentation using cascaded anisotropic convolutional neural networks", Lecture Notes in Computer Science (including subseries Lecture Notes in Artificial Intelligence and Lecture Notes in Bioinformatics), Vol. 10670, Pages 178–190, 2018.

20. Diaz, I. et al., "An automatic brain tumor segmentation tool", Proceedings of the Annual International Conference of the IEEE Engineering in Medicine and Biology Society, Osaca, Pages 3339-3342, 2013.

21. Liu, J. et al., "A survey of MRI-based brain tumor segmentation methods", Tsinghua Science and Technology, Vol. 19, Issue 6, Pages 578-595, 2014.

22. Chen, W., Liu, B., Peng, S., Sun, J. & Qiao, X., "S3D-UNET: Separable 3D U-Net for brain tumor segmentation", Lecture Notes in Computer Science (including subseries Lecture Notes in Artificial Intelligence and Lecture Notes in Bioinformatics), Vol. 11384, Pages 358-368, 2019.

23. Dong, H., Yang, G., Liu, F., Mo, Y. & Guo, Y., "Automatic Brain Tumor Detection and Segmentation Using U-Net Based Fully Convolutional Networks", Communications in Computer and Information Science, Vol. 723, Pages 506–517, Springer, Cham, 2017.

24. Myronenko, A., "3D MRI brain tumor segmentation using autoencoder regularization", Lecture Notes in Computer Science (including subseries Lecture Notes in Artificial Intelligence and Lecture Notes in Bioinformatics), Vol. 11384, Pages 311-320, 2019.

25. Lachinov, D., Vasiliev, E. & Turlapov, V., "Glioma segmentation with cascaded UNet", Lecture Notes in Computer Science (including subseries Lecture Notes in Artificial Intelligence and Lecture Notes in Bioinformatics), Cham: Springer International Publishing, Pages 189-198, 2018.

26. Ronneberger, O., Fischer, P. & Brox, T., "U-net: Convolutional networks for biomedical image segmentation", Lecture Notes in Computer Science (including subseries Lecture Notes in Artificial Intelligence and Lecture Notes in Bioinformatics), Vol. 9351, Pages 234–241, 2015.

27. Antonelli, M. et al., "The Medical Segmentation Decathlon", Nature Communications, Vol. 13, Issue 1, Pages 1-13, 2022.

28. "Medical Segmentation Decathlon", http://medicaldecathlon.com/, June 06, 2023.

29. Diederik, K. & Ba, J. L. "ADAM: A Method for Stochastic Optimization", arXiv preprint arXiv:1412.6980, 2014.

30. Ronneberger O, Fischer P, Brox T., "U-net: Convolutional networks for biomedical image segmentation", Lecture Notes in Computer Science (including subseries Lecture Notes in Artificial Intelligence and Lecture Notes in Bioinformatics), Vol. 9351, Pages 234–241, 2015.

31. Krizhevsky, A., Sutskever, I. & Hinton, G. E., "ImageNet classification with deep convolutional neural networks", Commun ACM, Vol. 60, Issue 6, Pages 84-90, 2017.

32. Dice, L. R., "Measures of the Amount of Ecologic Association Between Species", Ecology, Vol. 26, Issue 3, Pages 297-302, 1945.

33. Li, H., Li, A. & Wang, M., "A novel end-to-end brain tumor segmentation method using improved fully convolutional networks", Comput Biol Med, Vol. 108, Pages 150-160, 2019.

34. Taha, A. A. & Hanbury, A., "Metrics for evaluating 3D medical image segmentation: Analysis, selection, and tool", BMC Med Imaging, Vol. 15, Issue 1, Pages 1-28, 2015.

35. Havaei, M. et al., "Brain tumor segmentation with Deep Neural Networks", Medical Image Analysis, Vol. 35, Pages 18–31, 2017.

36. Kamnitsas, K. et al., "Efficient multi-scale 3D CNN with fully connected CRF for accurate brain lesion segmentation" ,Medical Image Analysis, Vol. 36, Pages 61–78, 2017.

37. Shreyas, V. & Pankajakshan, V., "A deep learning architecture for brain tumor segmentation in MRI images", 2017 IEEE 19th International Workshop on Multimedia Signal Processing (MMSP), Luton, Pages 1–6, 2017.

38. Kong, X., Sun, G., Wu, Q., Liu, J. & Lin, F., "Hybrid pyramid u-net model for brain tumor segmentation", IFIP Advances in Information and Communication Technology, Springer, Cham., Vol. 538, Pages 346–355, 2018.

39. Chen, S., Ding, C. & Liu, M., "Dual-force convolutional neural networks for accurate brain tumor segmentation", Pattern Recognit, Vol. 88, Pages 90–100, 2019.

40. Tan, L., Ma, W., Xia, J. & Sarker, S., "Multimodal Magnetic Resonance Image Brain Tumor Segmentation Based on ACU-Net Network", IEEE Access, Vol. 9, Pages 14608–14618, 2021.

41. Kausar, A., Razzak, I., Shapiai, I. & Alshammari, R., "An Improved Dense V-Network for Fast and Precise Segmentation of Left Atrium", 2021 International Joint Conference on Neural Networks (IJCNN), Shenzhen, Pages 1-8, 2021.

42. Chakravarty, A. & Sivaswamy, J., "RACE-Net: A Recurrent Neural Network for Biomedical Image Segmentation", IEEE J Biomed Health Inform, Vol. 23, Issue 3, Pages 1151–1162, 2019.